Article

Pd-Supported Co$_3$O$_4$/C Catalysts as Promising Electrocatalytic Materials for Oxygen Reduction Reaction

Virginija Kepenienė [1,*], Raminta Stagniūnaitė [1], Sidra Rafique [1], Jūratė Vaičiūnienė [1], Vitalija Jasulaitiene [1], Vidas Pakštas [1], Zita Sukackienė [1], Rasa Vilkauskaite [2], Loreta Tamašauskaitė-Tamašiūnaitė [1] and Eugenijus Norkus [1]

[1] Department of Catalysis, Center for Physical Sciences and Technology (FTMC), Saulėtekio Ave. 3, LT-10257 Vilnius, Lithuania

[2] Department of Chemistry and Bioengineering, Vilnius Gediminas Technical University, Sauletekio Ave. 11, LT-10223 Vilnius, Lithuania

[*] Correspondence: virginija.kepeniene@ftmc.lt; Tel.: +370-5-264-8845; Fax: +370-5-264-9774

Abstract: This paper describes the activity of PdCo$_3$O$_4$/C obtained by wet impregnation towards the oxygen reduction reaction (ORR). For this purpose, the Co$_3$O$_4$/C substrate was synthesized using the microwave irradiation heating method with further annealing of the substrate at 400 °C for 3 h (Co$_3$O$_4$/C-T). Then, the initial Co$_3$O$_4$/C substrate was impregnated with palladium chloride (Pd-Cl$_2$-Co$_3$O$_4$/C), and then part of the obtained Pd-Cl$_2$-Co$_3$O$_4$/C catalyst was annealed at 400 °C for 3 h (PdOCo$_3$O$_4$/C). The electrocatalytic activity of the prepared catalysts was investigated for the oxygen reduction reaction in alkaline media and compared with the commercial Pt/C (Tanaka wt. 46.6% Pt) catalyst. It was found that the annealed PdOCo$_3$O$_4$/C catalyst showed the largest ORR current density value of -11.27 mA cm^{-2} compared with Pd-Cl$_2$-Co$_3$O$_4$/C (-7.39 mA cm^{-2}) and commercial Pt/C (-5.25 mA cm^{-2}).

Keywords: palladium; cobalt oxide; nanoparticles; oxygen reduction; fuel cells

1. Introduction

Energy is one of the most important and necessary factors for progress in science and enhancing quality of human life. However, the issues surrounding the use of fossil fuels, in terms of air pollution and climate change, have been considered in the past few decades. The first scientist who said that fossil fuels might cause climate change was electrochemist Svante Arrhenius in the nineteenth century [1]. So, the depletion of the ozone layer, climate warming, and other pollution issues have increased the necessity for a cleaner and environmentally friendly mode of energy. That is why fuel cells have come to the forefront of the catalyst field [2]. Many types of fuel cells have been investigated with the aim of finding one of the best alternatives, a cleaner and more effective energy resource, which can work intermediately without any mechanical link. In particular, the final products of fuel cell reactions are friendlier to the environment. Depending on the fuel used, the products of working fuel cells are H$_2$O for hydrogen fuel cells and H$_2$O and CO$_2$ for liquid fuel cells using an alcohol solution. Although it sounds promising, there are some questions scientists have been faced with. One of them regards efficient materials, which are used in the anodic and cathodic sides of the fuel cell. It is well-known that Pt is one of the best and most effective catalysts used in fuel cells [3]. However, recent research has focused on platinum-free materials or at least on the creation of electroactive materials with a reduced amount of Pt, and thus with increased activity of the catalyst. Oxygen (usually from air) is commonly used at the cathodic side of the fuel cell because it has good reduction potential and is highly abundant in the environment. The catalyst used as a cathode material has to be efficient and selective for the oxygen reduction reaction to achieve the highest device performance. Moreover, as mentioned before, it is important to find alternative catalysts

that are less expensive and more catalytically active than bare Pt. Recent research has focused on metals such as Mn, Fe, Co, Ni, Zn, etc., and hydroxides/oxides/dichalcogenides because of their ability to synergistically improve the electrochemical performance due to their flexible oxidation states [4–9]. Furthermore, transition-metal oxides are attractive electrocatalytic materials because of their high stability. One of the most promising electrocatalysts is Co_3O_4 due to its low cost, availability, stability, and electrocatalytic activity towards the oxygen reduction reaction in alkaline media [6–8]. Recently, nanostructured metal oxides have attracted attention because of their application in electronics and other industries. In addition to this, nanostructured Co_3O_4 is distinguished from other metal oxides because of its unique magnetic and optical properties. Moreover, it can be an attractive electrocatalytic material because of its defined electrochemical redox activity, stable chemical state, and low cost [10]. Cobalt(II,III) oxide, Co_3O_4, is described as a promising electrocatalyst for ORR, and its electrocatalytic properties can be further improved by developing its different morphologies [5]. There are many different morphologies of Co_3O_4, such as nanotubes, nanowalls, nanosheets, nanocubes, nanoboxes, microspheres, flower-like structures, etc., which have different properties and depend on the method of Co_3O_4 preparation used [11–15]. Hexamethylenetetramine (HMTA) is known as a cheap, ecofriendly, and readily available heterocyclic organic compound with a cage-like structure using a metal–HMTA complex precursor for synthesis of metal oxide nanoparticles [16]. W. Jia et al. described the influence of HMT on the significant morphological evolution of Co_3O_4. Depending on the mole ratio of HMT in the synthesis, different structures of Co_3O_4 can be obtained, such as nanosheets accompanied by a large number of spherical nanoparticles → some strip-like particles due to the agglomeration of spherical nanoparticles → nanosheets resulting from the growth of strip-like particles → coarse flower-like particles owing to the connection among the nanosheets → and nanosheets gradually covered with flower-like particles [17]. Moreover, the particle size decreases with increased HMT concentrations [18]. However, the efficiency of individual transition-metal oxides is commonly poor; therefore, Co_3O_4 is usually used as a substrate and combined with other conductive materials to improve the electrocatalytic performance [19,20]. Pd has attracted much attention because of its similarity to Pt, in both its atomic size and crystal structure. However, bare Pd catalysts show lower activity towards the ORR compared with bare Pt catalysts, but some supplements, such as transition metals or metal oxides, improve the catalytic properties of palladium [21–24]. Furthermore, it is very attractive due to its cost, which is three times lower than that of Pt. In addition to this, adding metal oxides, such as Co_3O_4, increases the oxygen transfer to Pd, which also increases the electrocatalytic activity of catalysts [25–27].

In this work, Co_3O_4/C and Pd-supported Co_3O_4/C catalysts were prepared using two methods—microwave irradiation heating and wet impregnation. First, the Co_3O_4/C substrate was prepared using the microwave heating method. Furthermore, the substrate was impregnated with palladium, and a Pd-supported Co_3O_4/C catalyst was obtained. Then, both the Co_3O_4/C substrate and the impregnated Pd-Cl_2-Co_3O_4/C catalyst were annealed at 400 °C for 3 h, and Co_3O_4/C-T and PdOCo_3O_4/C catalysts were obtained.

The composition, morphology, and structure of the prepared materials were characterized using inductively coupled plasma optical emission spectroscopy (ICP-OES), field-emission scanning electron microscopy (FESEM), transmission electron microscopy (TEM), X-ray diffraction (XRD), and X-ray photoelectron spectroscopy (XPS). We investigated the electrocatalytic properties of the prepared catalysts during an oxygen reduction reaction in alkaline media using rotating disk electrode (RDE) linear sweep voltammetry (LSV) and compared them to those of the commercial Pt/C catalyst.

It was determined that the annealed PdOCo_3O_4/C catalyst showed the highest electrocatalytic activity, the most positive onset potential, and the largest current density towards the oxygen reduction reaction in an alkaline medium as compared with the other obtained catalysts.

2. Results

Table 1 depicts the results, which were obtained after the physical characterization of the synthesized Co_3O_4/C, Co_3O_4/C-T, Pd-Cl_2-Co_3O_4/C, and $PdOCo_3O_4/C$ catalysts and commercial Pt/C. The amount of Pt, Pd, and Co for each catalyst was determined by ICP-OES. The calculated mass weight of Co_3O_4 was ca. 58 and 74 wt.% in the Co_3O_4/C and Co_3O_4/C-T catalysts, respectively (Table 1). $PdCl_2$ and Co_3O_4 mass weight in the $PdCl_2$-Co_3O_4/C catalyst was ca. 7.7 and 22.5 wt.%, respectively. In the case of the $PdOCo_3O_4/C$ catalyst, PdO and Co_3O_4 mass weight was ca. 3.03 and 12.46 wt.%, respectively. For electrochemical measurements, estimated Co loading in the catalysts varied from ca. 54 to ca. 270 $\mu g\ cm^{-2}$. Loading of Pd was equal to 47.05 and 83.00 $\mu g\ cm^{-2}$ in the synthesized $PdOCo_3O_4/C$ and Pd-Cl_2-Co_3O_4/C catalysts, respectively. In the commercial Pt/C catalyst, Pt loading was equal to 118.04 $\mu g\ cm^{-2}$ (Table 1).

Table 1. Physical characterization of the investigated catalysts.

Catalyst	Loading, $\mu g\ cm^{-2}$			Mass Weight, wt.%		ESA	
	Pt	**Pd**	**Co**	**$PdCl_2$/PdO**	**Co_3O_4**	**cm^{-2}**	**$m^2\ g^{-1}$**
Co_3O_4/C	-	-	254.29	-	58	-	-
Co_3O_4/C-T	-	-	273.48	-	74	-	-
Pd-Cl_2-Co_3O_4/C	-	83.00	98.43	7.7	22.5	0.34	10.04
$PdOCo_3O_4/C$		47.05	54.46	3.03	12.46	2.54	74.97
Pt/C	118.40	-	-	-	-	11.04	47.52

Electrochemically active surface areas (ESAs) of the investigated Pt/C, Pd-Cl_2-Co_3O_4/C, and $PdOCo_3O_4/C$ catalysts were determined from cyclic voltammograms (CVs) recorded in the argon-deaerated 0.5 M H_2SO_4 solution at a sweep rate of 50 mV s^{-1} (Figure 1). The ESA value for Pt/C was calculated by integrating the area of the peak associated with the hydrogen adsorption region (Q_H) with a charge density of 210 $\mu C\ cm^{-2}$. ESAs of Pd in Pd-Cl_2-Co_3O_4/C and $PdOCo_3O_4/C$ catalysts involved the utilization of a value of 424 $\mu C\ cm^{-2}$ as the charge density associated with the reduction of PdO at a potential range of 0.5–0.7 V vs. the reversible hydrogen electrode (RHE) [28,29]. The results obtained are presented in Table 1.
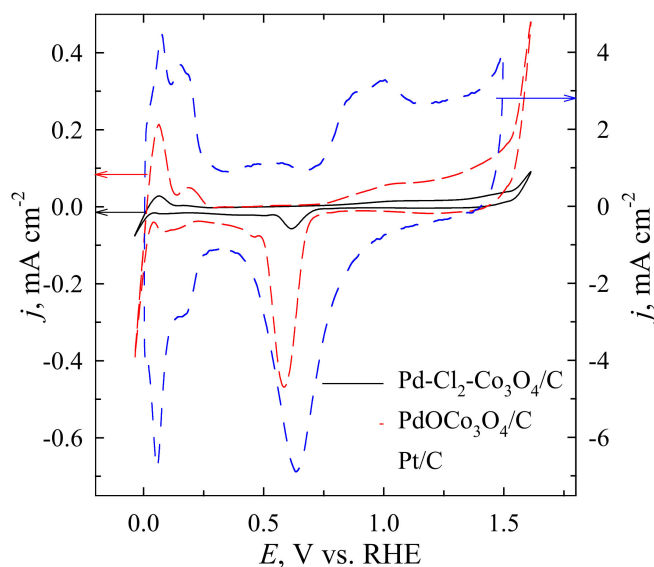

Figure 1. CVs of the investigated catalysts recorded in an Ar-deaerated 0.5 M H_2SO_4 solution at 50 mV s^{-1}.

The crystal structure of the obtained catalysts was further characterized by XRD as shown in Figure 2. All the profiles are consistent with a hexagonal graphite-2H phase (ICDD #00-056-0160) as a base for the synthesized material (Figure 2, marked as C). The intense diffraction peaks seen at $2\Theta = 16.15, 18.34, 39.25$, and $53.55°$ in the Co_3O_4/C (Figure 2a, Pattern 1) and $Pd-Cl_2-Co_3O_4/C$ (Figure 2b, Pattern 1) profiles can be attributed to the (101), (003), (024), and (220) crystallographic planes of trigonal $Co_2Cl(OH)_3$ (ICDD #04-011-5213) with crystallites size of about 12 nm (Figure 2a,b, Pattern 1). During the annealing in an air atmosphere at a temperature of 400 °C, the structure of $Co_2Cl(OH)_3$ changed to the cubic structure of Co_3O_4 (ICDD #01-078-1969). The $Co_3O_4/C-T$ (Figure 2a, Pattern 2) and $PdOCo_3O_4/C$ (Figure 2b, Pattern 2) profiles show the diffraction peaks obtained at $2\Theta = 19.00, 31.27, 44.80, 59.35$, and $65.22°$, attributed to the crystallographic planes (111), (220), (400), (511), and (440), respectively, of the cubic structure of Co_3O_4 (Figure 2a,b Pattern 2). The size of Co_3O_4 crystallites was calculated as 18.1 ± 0.4 nm and 13.8 ± 0.5 nm for $Co_3O_4/C-T$ and $PdOCo_3O_4/C$, respectively (Table 2). Pd may have possibly affected the formation of finer derivatives and thus the formation of a more active particle surface. As well as after annealing, a broad tetragonal PdO peak (ICDD #01-086-4074) appears in the XRD pattern of the $PdOCo_3O_4/C$ catalyst (Figure 2b, Pattern 2). This diffraction peak is quite broad, indicating fine-phase crystallinity. PdO crystallites about 4 nm in size were detected in the $PdOCo_3O_4/C$ catalyst.
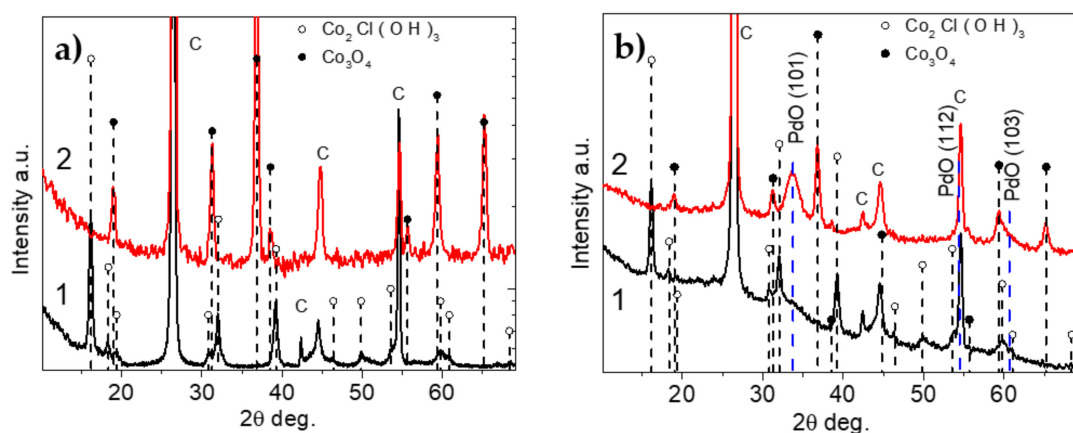

Figure 2. X-ray diffractograms for prepared samples. Pattern 1, immediately after synthesis: Co_3O_4/C (**a**), $Pd-Cl_2-Co_3O_4/C$ (**b**); Pattern 2, after annealing at a temperature of 400 °C for 3 h: $Co_3O_4/C-T$ (**a**), $PdOCo_3O_4/C$ (**b**).

Table 2. The size of Pd, Co, and Pt crystallites (XRD) and particles (TEM) in the investigated catalysts.

Catalyst	Crystallite—Average Size Value, nm		
	XRD		TEM
	PdO/Pt	Co_3O_4	
Co_3O_4/C	-	~12.0	~25.0
$Co_3O_4/C-T$	-	18.1 ± 0.4	~25.0
$Pd-Cl_2-Co_3O_4/C$	-	~12.0	~6.0
$PdOCo_3O_4/C$	4.0	13.8 ± 0.5	~3.0–44
Pt/C	4–5 [30]	-	4–5 [30]

SEM images present the surface morphology of all the prepared Co_3O_4/C and Pd-supported Co_3O_4/C powders. It can be seen that the $Co_2Cl(OH)_3$ and Co_3O_4 nanoparticles had cubic shapes and were distributed in small groups on a carbon surface for all investigated samples (Figure 3a–d). As seen in the $PdOCo_3O_4/C$ image (Figure 3d), very small spherical PdO nanoparticles were distributed on the surface.

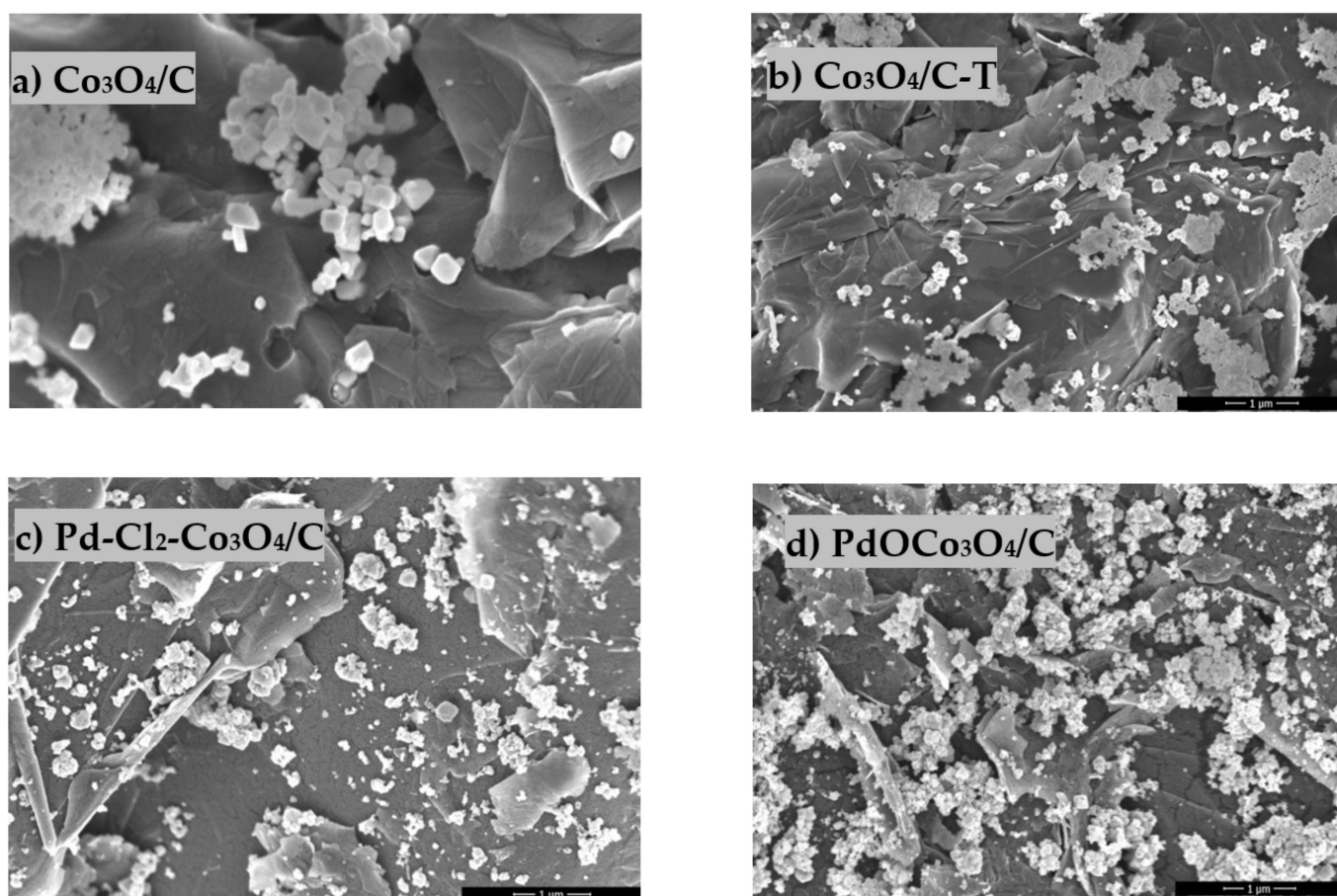**Figure 3.** SEM images of the Co_3O_4/C (**a**), Co_3O_4/C-T (**b**), Pd-Cl_2-Co_3O_4/C (**c**), and PdOCo_3O_4/C (**d**) catalysts.

The size of nanoparticles obtained in the Co_3O_4/C, Pd-Cl_2-Co_3O_4/C, Co_3O_4/C-T, and PdOCo_3O_4/C catalysts was estimated from TEM images (Figure 4a–d). The calculated size of nanoparticles is given in Table 2. Furthermore, EDX analysis of TEM confirmed the presence of $PdCl_2$ and PdO. The TEM images agree with the SEM images. It can be seen that $Co_2Cl(OH)_3$ and Co_3O_4 nanoparticles settled in groups and agglomerated (Figure 4a–d), and PdO nanoparticles were very small and covered the entire surface of the PdOCo_3O_4/C catalyst (Figure 4d).

The XPS studies of the Pd-Cl_2-Co_3O_4/C and PdOCo_3O_4/C catalysts overlapped with the other structural analysis methods used. Table 3 presents the binding energy (BE) values of the main spin-orbital splitting peak of Pd3d, Co2p, O1s, and C1s spectra. The Pd3d XPS spectra obtained for the Pd-Cl_2-Co_3O_4/C and PdOCo_3O_4/C catalysts are shown in Figure 5a,b, whereas the Co2p XPS spectra for those catalysts are represented in Figure 5c,d. The analysis of those XPS spectra revealed the coexistence of two doublets in the Pd3d spectra. $Pd3d_{5/2}$ peaks situated at 338.28 and 337.11 eV and their corresponding $Pd3d_{3/2}$ peaks at 343.64 and 342.42 eV, respectively, can be attributed to the chemical state of $PdCl_2$ and PdO (Figure 5a,b) [31,32]. For both catalysts, the obtained binding energies of about 780.15 and 779.55 eV assigned to the Co $2p_{3/2}$ transition were associated with Co^{3+} [31,33–36] lattice oxygen species (Figure 5c,d) [37]. The higher BE peaks of O1s XPS spectra, located at about 532–535 eV, are usually attributed to the presence of the surface of adsorbed O_2, H_2O, and CO_2 [37]. According to the XPS data, in the annealed PdOCo_3O_4/C catalyst, O_2 dominated in lattice oxygen species, indicating the Co_3O_4 phase in this catalyst. In the case of the Pd-Cl_2-Co_3O_4/C catalyst, oxygen was more likely to appear in the OH^- form or be adsorbed on a surface. These data confirm the results of XRD analysis, showing

that after annealing, $Co_2Cl(OH)_3$ changes to Co_3O_4. For both catalysts at a binding energy of about 284.2 eV in C1s distribution, the highest amount of carbon was estimated [38].
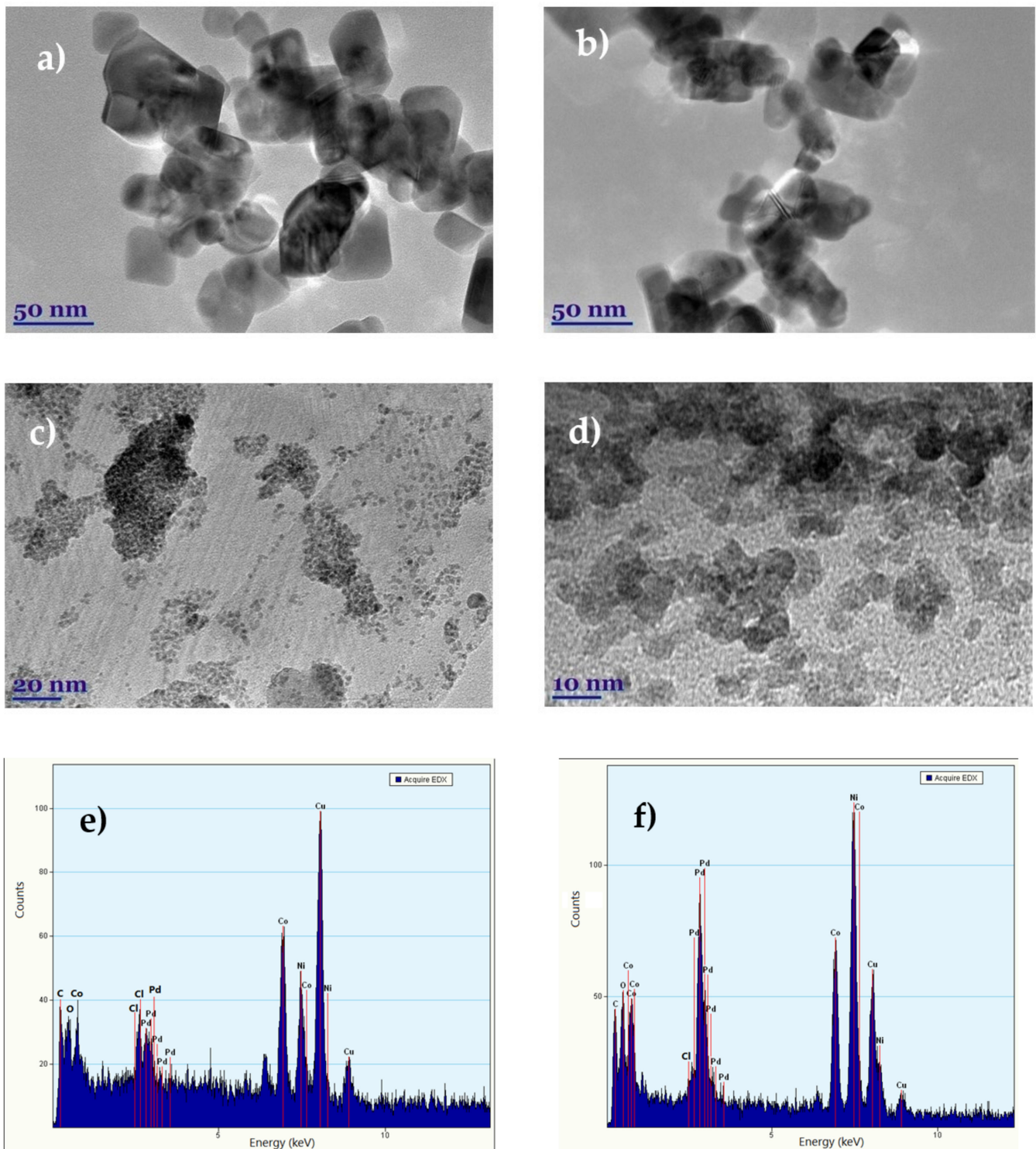

Figure 4. TEM images of the Co_3O_4/C (**a**), Co_3O_4/C-T (**b**), Pd-Cl_2-Co_3O_4/C (**c**), and $PdOCo_3O_4/C$ (**d**) catalysts. EDX analysis of Pd-Cl_2-Co_3O_4/C (**e**) and $PdOCo_3O_4/C$ (**f**) catalysts.

Table 3. Data from XPS analysis.

Catalyst	Pd3d$_{5/2}$		Pd3d$_{3/2}$		Co2p$_{3/2}$		O1s		C1s	
	E$_b$, eV	at.%	E$_b$, eV	at.%	E$_b$, eV	at.%	E$_b$, eV	at.%	E$_b$, eV	at.%
Pd-Cl$_2$-Co$_3$O$_4$/C	338.28	65.63	343.63	34.37	780.15	41.64	529.91	29.42	284.26	50.25
					783.09	39.13	531.86	24.35	284.87	28.16
					786.30	19.23	532.82	19.98	286.41	14.64
							533.92	26.25	287.73	6.95
PdOCo$_3$O$_4$/C	337.11	67.93	342.42	32.07	779.55	57.03	529.70	8.39	284.19	34.73
					782.22	28.19	531.27	24.84	284.54	24.46
					786.17	14.78	532.69	44.72	285.84	26.36
							533.98	17.82	286.94	11.74
							535.03	3.22	288.49	2.71

Furthermore, the electrocatalytic activity of as-prepared catalysts was investigated for the oxygen reduction reaction against the commercial Pt/C. Figure 6 shows the ORR polarization curves recorded in the O$_2$-saturated 0.1 M NaOH solution. The electrode potential was scanned from 1.0 V in the cathodic direction to 0.2 V vs. the RHE at a scan rate of 5 mV s^{-1}. The rotation speed was varied from 400 to 2000 rpm (Figure 6a–e). From the obtained data, it can be seen that all catalysts demonstrated a typical view of ORR curves with the onset potentials range of 0.77–0.95 V vs. the RHE. According to the literature, the oxygen reduction reaction occurs at the potential range between 0.7 and 1.0 V vs. the RHE [28,39]. It can be seen that, as expected, the highest activity for the ORR of the investigated as-prepared catalysts was shown by the annealed PdOCo$_3$O$_4$/C catalyst (Figure 6d) with the onset potential of 0.92 V vs. the RHE, which also showed the largest maximum current density at -11.27 mA cm^{-2}, as compared with the Pd-Cl$_2$-Co$_3$O$_4$/C catalyst, with the onset potential of 0.91 V and a limiting current density of -7.39 mA cm^{-2} (Figure 6c). In the case of non-Pd catalysts, the annealed Co$_3$O$_4$/C-T showed a more negative ORR onset potential of 0.83 V (Figure 6b), and the freshly prepared Co$_3$O$_4$/C catalyst exhibited the most negative ORR onset value at 0.78 V (Figure 6a). The polarization curves of commercial Pt/C showed the most positive onset potential at 0.95 V, but a lower limiting current density value of -5.25 mA cm^{-2} compared with Pd-supported Co$_3$O$_4$/C catalysts (Figure 5e). The data obtained show that the PdOCo$_3$O$_4$/C catalyst exhibited a very similar onset potential to Pt/C.
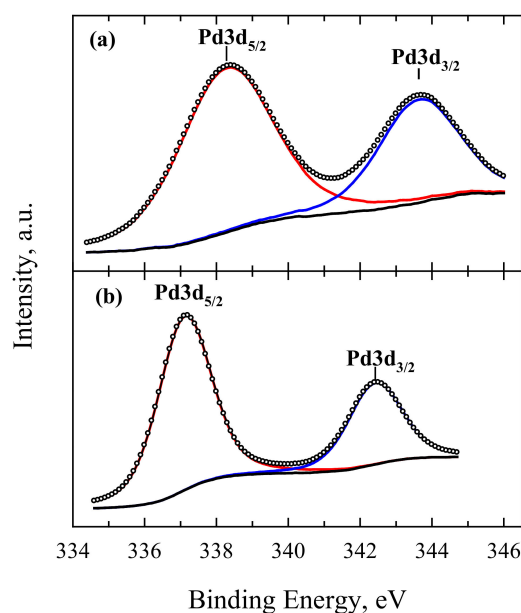
Figure 5. *Cont.*
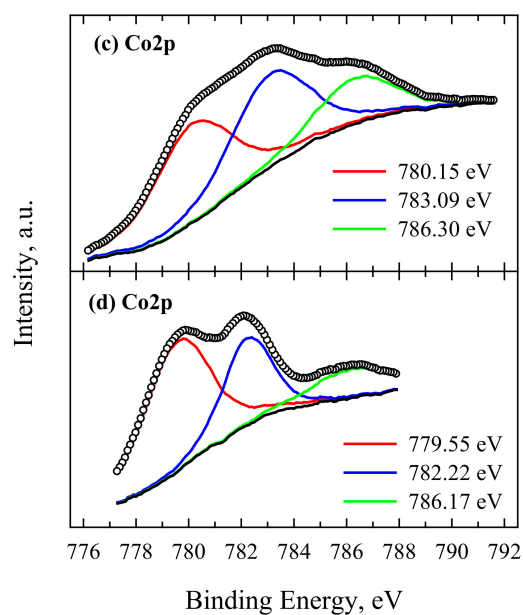
Figure 5. Pd3d XPS spectra for Pd-Cl$_2$-Co$_3$O$_4$/C (**a**) and PdOCo$_3$O$_4$/C (**b**) catalysts. (**c**,**d**) Co2p XPS spectra for Pd-Cl$_2$-Co$_3$O$_4$/C and PdOCo$_3$O$_4$/C, respectively.
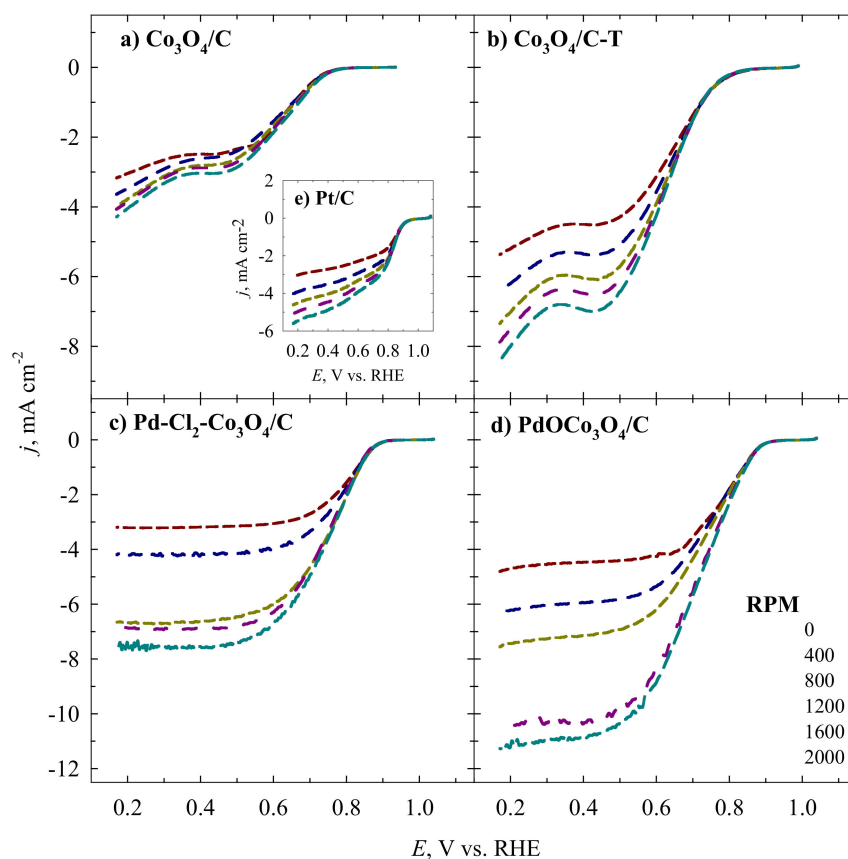
Figure 6. Linear sweep voltammetry curves for O$_2$ reduction on the Co$_3$O$_4$/C (**a**), Co$_3$O$_4$/C-T (**b**), Pd-Cl$_2$-Co$_3$O$_4$/C (**c**), PdOCo$_3$O$_4$/C (**d**), catalysts in the O$_2$-saturated 0.1 M NaOH solution at 5 mV s^{-1}.

Figure 7 reveals this similarity more clearly. Figure 7a compares the LSV curves of all investigated catalysts at 1600 rpm in the O_2-saturated 0.1 M NaOH solution. It can be seen that the effect of the beginning of the ORR on the Pd-Cl_2-Co_3O_4/C, PdOCo_3O_4/C, and Pt/C catalysts was very similar, and these three catalysts were significantly more active than Co_3O_4/C and Co_3O_4/C-T. The initial current density for the ORR at 0.9 and 0.85 V was higher on the Pt/C (-1.296 and -2.832 mA cm^{-2}, respectively) than on PdOCo_3O_4/C (-0.142 and -0.852 mA cm^{-2}). Furthermore, at the potential of 0.8 V, the current density increased for both Pt/C and PdOCo_3O_4/C catalysts up to about -3.990 and -2.224 mA cm^{-2}. Then, the current density for PdOCo_3O_4/C increased as the potential became more negative, and at 0.7 V, the current density for the ORR on PdOCo_3O_4/C was -5.551 mA cm^{-2}, which was ca. 1.2 times higher than on the commercial Pt/C catalyst at the same voltage with a current density value of -4.781 mA cm^{-2} (Figure 7a). Hence, according to LSV measurements, the ORR activity over the catalysts followed the order of Co_3O_4/C < Co_3O_4/C-T < Pd-Cl_2-Co_3O_4/C < PdOCo_3O_4/C ≤ Pt/C.
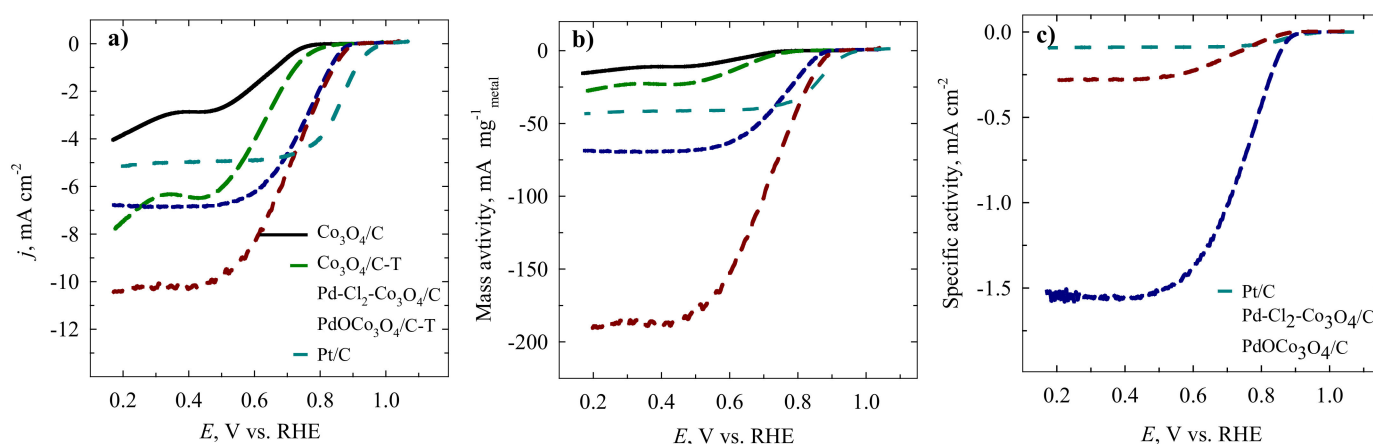

Figure 7. Comparison of ORR current densities at 1600 rpm in an O_2-saturated 0.1 M NaOH solution (**a**), ORR current densities normalized by the metal loading (**b**), and ORR current normalized by the ESA values (**c**) for all investigated catalysts.

Regarding limiting current density, Pd-Cl_2-Co_3O_4/C and PdOCo_3O_4/C demonstrated higher current densities, outperforming Pt/C, Co_3O_4/C and Co_3O_4/C-T catalysts. As the rotation rate is the same, the amount of oxygen being supplied to the working electrode is also the same; the only determining factor of the limiting current density is the efficiency of the reaction. Higher limiting current densities indicate a higher selectivity for the four-electron reduction to water on the Pd-Cl_2-Co_3O_4/C and PdOCo_3O_4/C catalysts.

When the current densities of LSV curves at 1600 rpm were normalized by loading of Pd, Pt, and Co (in the case of Pd-free catalysts), this tendency became clearer (Figure 7b). It was found that the largest mass activity of -101.85 mA mg$_{Pd}^{-1}$ at 0.7 V was exhibited by the annealed PdOCo_3O_4/C catalyst, which was about 2 times higher than that of the impregnated Pd-Cl_2-Co_3O_4/C catalyst (-47.63 mA mg$_{Pd}^{-1}$) and 5.4 times higher as compared to that of the commercial Pt/C catalyst (-18.77 mA mg$_{Pt}^{-1}$). Undoubtedly, the Co_3O_4/C and Co_3O_4/C-T catalysts showed the lowest ORR mass activity at 0.7 V of -2.27 and -5.39 mA mg$_{Co}^{-1}$, respectively. Calculating the mass activity of the investigated catalysts at 0.8 V, the tendency remained the same: the mass activity of as-prepared catalysts increased in the order of Co_3O_4/C (-0.096 mA mg$_{Co}^{-1}$) < Co_3O_4/C-T (-0.826 mA mg$_{Co}^{-1}$) < Pt/C (-15.666 mA mg$_{Pt}^{-1}$) Pd-Cl_2-Co_3O_4/C (-18.350 mA mg$_{Pd}^{-1}$) < PdOCo_3O_4/C (-38.121 mA mg$_{Pd}^{-1}$). When currents of LSV measurements were normalized by the ESA values of Pd and Pt at 0.8 V, the highest specific activity was exhibited by the as-prepared Pd-Cl_2-Co_3O_4/C (-0.405 mA cm^{-2}) catalyst compared with the PdOCo_3O_4/C (-0.057 mA cm^{-2}) and Pt/C (-0.071 mA cm^{-2}) catalysts. The tendency remained the same at 0.7 V: the highest specific activity was exhibited by the Pd-Cl_2-Co_3O_4/C cata-

lyst (-1.028 mA cm^{-2}) compared with the PdOCo$_3$O$_4$/C (-0.153 mA cm^{-2}) and Pt/C (-0.085 mA cm^{-2}) catalysts. Density functional theory suggests that high ORR activity may arise from appropriate oxygen adsorption strength at the interface of PdO-Co$_3$O$_4$.

Hereinafter, the durability test of as-prepared catalysts was carried out by chronoamperometry measurements at a potential value of 0.55 V for the 1900s (Figure 8a). It can be seen that after approximately 200–400 s, the current density settled down and only slightly increased over time. Figure 8b presents the normalized ORR current densities (%) for each catalyst after stabilization of current density during the process. It was calculated that the investigated catalysts maintained 78, 83, 90, 92, and 95% of their initial efficiency in the order of Co$_3$O$_4$/C < Co$_3$O$_4$/C-T < Pd-Cl$_2$-Co$_3$O$_4$/C < PdOCo$_3$O$_4$/C $\leq$ Pt/C.
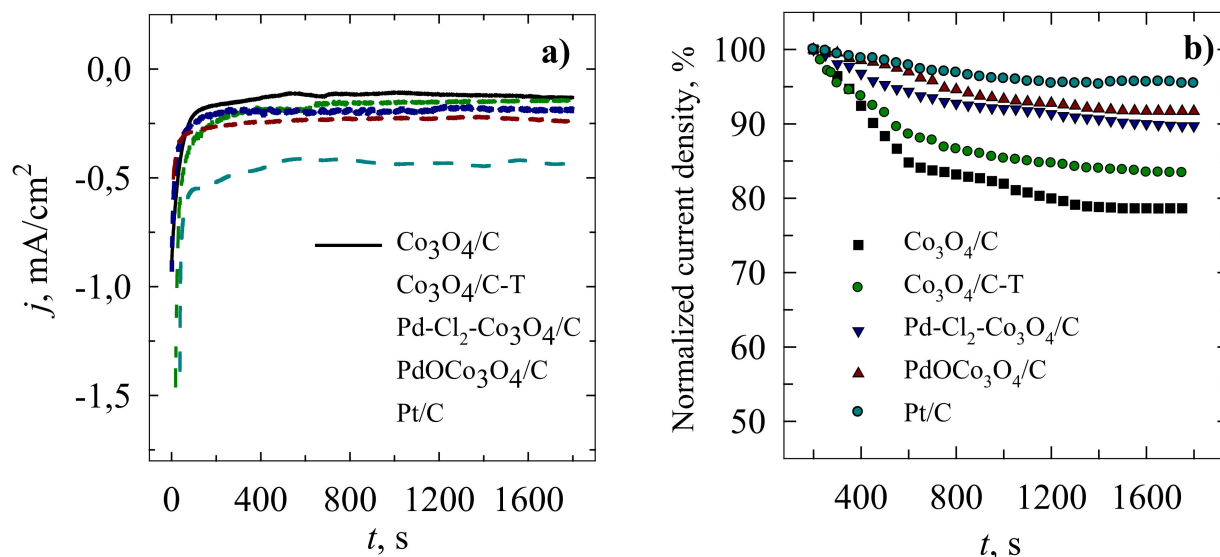

Figure 8. Chronoamperometric curves recorded on the investigated catalysts at 0.55 V in an O$_2$-saturated 0.1 M NaOH solution: (**a**) chronoamperometric responses (percentage of current density retained vs. operation time) of all the catalysts (**b**).

It is worth noting that the PdOCo$_3$O$_4$/C catalyst, having a three-times-lower noble metal loading, demonstrated similar stability to the commercial Pt/C during the ORR process in an alkaline medium.

Koutecky–Levich (K-L) plots were generated from the LSV curves where the inverse current density taken at 0.65, 0.7, 0.75, and 0.8 V was plotted against the inverse square root of rotation speed (Figure 9). The K-L curves show a linear relationship between j^{-1} and $w^{-1/2}$, indicating the first-order dependence of the ORR kinetics at different potentials (0.65–0.80 V) for all investigated catalysts. However, the calculated number of electrons transferred (n) varied from two to four, indicating a 2e$^-$ transfer reaction for Co$_3$O$_4$/C catalysts when the reduction of O$_2$ produced HO$_2^-$ and OH$^-$ [40] and a 4 e$^-$ transfer reaction and direct reduction of O$_2$ to H$_2$O [41] on the surfaces of Pd-Cl$_2$-Co$_3$O$_4$/C and PdOCo$_3$O$_4$/C catalysts.

Moreover, we compared the electrocatalytic activity of our prepared catalysts towards the ORR with other Pd- and Co-supported catalysts recently reported in the literature. Table 4 presents the data collected. It can be seen that according to the onset potential of the ORR, the as-prepared Co$_3$O$_4$/C, Co$_3$O$_4$/C-T, Pd-Cl$_2$-Co$_3$O$_4$/C, and PdOCo$_3$O$_4$/C catalysts exhibited very similar or even higher electrocatalytic activity towards the ORR in alkaline media compared to that stated in the literature.
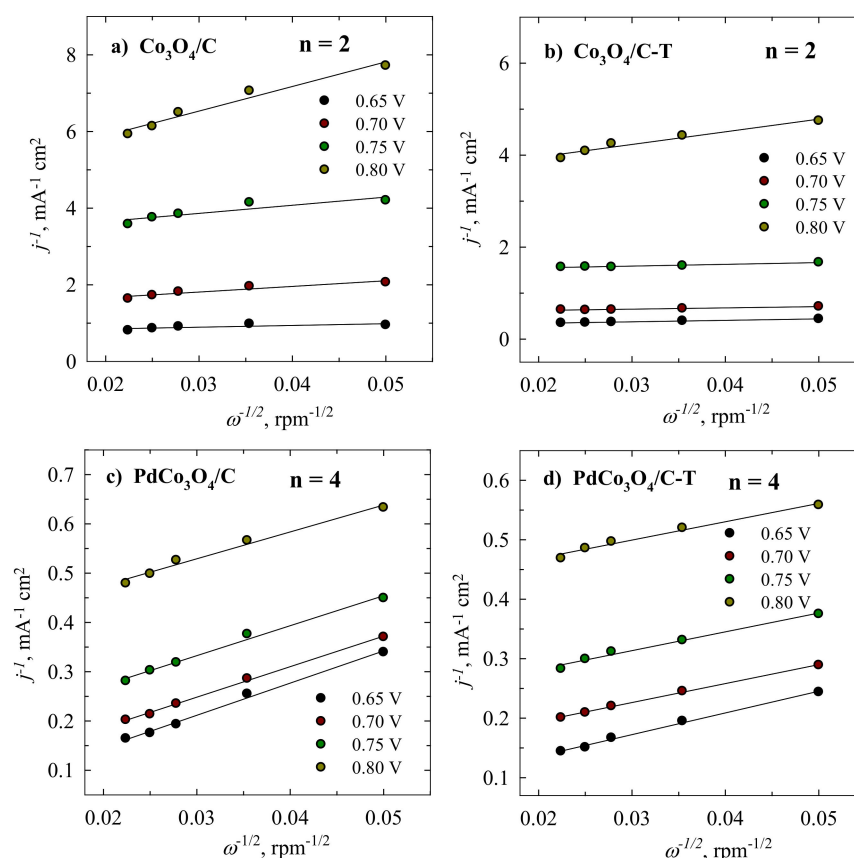
Figure 9. Koutecky–Levich plots of the investigated catalysts at different potentials in an O_2-saturated 0.1 M NaOH solution.

Table 4. The comparison of potentials of various catalysts.

Catalyst	E_{onset}, V vs. RHE	$E_{half-wave}$ V vs. RHE	Electrolyte	References
Co_3O_4/C	0.78	0.62	0.1 M NaOH	This work
Co_3O_4/C-T	0.83	0.63	0.1 M NaOH	This work
Pd-Cl_2-Co_3O_4/C	**0.91**	**0.75**	0.1 M NaOH	This work
PdOCo_3O_4/C	**0.92**	**0.72**	0.1 M NaOH	This work
Pt/C	0.95	0.86	0.1 M NaOH	This work
PdYNPs	0.90	0.85	0.1 M KOH	[42]
Pd_3Fe NPs/CB	0.90	Not presented	0.1 M NaOH	[8]
Pd_3Co NPs/CB	0.90	Not presented	0.1 M NaOH	[8]
Pd_3Ni NPs/CB	0.87	Not presented	0.1 M NaOH	[8]
Pd@Zncore shell	0.85	0.82	0.1 M KOH	[42]
Co_3O_4/C_{IMP-MW}	0.83	0.67	0.1 M NaOH	[19]
Co_3O_4/C	0.83	0.78	1 M KOH	[43]
PdCo-300	0.81	0.83	0.1 M KOH	[43]

3. Materials and Methods

3.1. Chemicals

$CoCl_2 \cdot 6H_2O$ (98%), NaCl ($\geq$99.0%), hexamethylenetetramine (HMT) (99–100.5%), graphite powder (99.9995%) (carbon (C) in the text), and $PdCl_2$ (99%) were purchased from Sigma-Aldrich and Alfa-Aesar Supplies. Polyvinylidene fluoride, N-methyl-2-pyrrolidone, ethanol (96%), H_2SO_4 (96%), and NaOH (98.8%) were purchased from Chempur Company. Argon and oxygen gases (99.999%) were used for the saturation of the NaOH solution. The commercial Pt/C was Tanaka wt. 46.6% Pt. All chemicals were of analytical grade. Ultra-pure water with a resistivity of 18.2 MΩ cm^{-1} was used for preparing the solutions.

3.2. Preparation of Catalysts

The Co_3O_4/C substrate was prepared as follows: (1) HMT, sodium chloride, and cobalt chloride salts were mixed together (the mass ratio being 4:2.5:1) with ethanol and water solution (the volume ratio being 5:1) and stirred for 15 min on the magnetic stirrer; (2) then, 30 mg of carbon was added to the mixture and stirred for 1 h. For microwave irradiation, a Monowave 300 microwave reactor (Anton Paar) was used. The synthesis of Co_3O_4 nanoparticles on carbon was carried out at a temperature of 120 °C for 4 h. After preparation, the synthesized catalyst was washed with ethanol and water solution (the volume ratio being 5:1), ultra-pure water, then filtered and dried in a vacuum oven at 80 °C for 2 h.

The obtained Co_3O_4/C substrate was impregnated with palladium chloride solution as follows: 20 mg of prepared Co_3O_4/C substrate was added to 6 mL of 0.25 g L^{-1} $PdCl_2$ solution and stirred for 30 min on a magnetic stirrer. After impregnation, the mixture was washed with ultra-pure water, then filtered and dried in a vacuum oven at 80 °C for 2 h. The $Pd-Cl_2-Co_3O_4/C$ catalyst was obtained.

Furthermore, the prepared Co_3O_4/C substrate and impregnated $Pd-Cl_2-Co_3O_4/C$ catalyst were annealed in an oven at 400 °C for 3 h in an air atmosphere, and catalysts denoted as $Co_3O_4/C-T$ and $PdOCo_3O_4/C$ were obtained.

3.3. Characterization of Catalysts

XRD patterns of studied catalysts were measured using an X-ray diffractometer Smart-Lab (Rigaku) equipped with an X-ray tube with a 9 kW rotating Cu anode. The measurements were performed using Bragg–Brentano geometry with a graphite monochromator on the diffracted beam and a step scan mode with a step size of 0.02 (in 2θ scale) and a counting time of 1 s per step. The measurements were conducted in the 2θ range of 10–75°. Phase identification was performed using the software package PDXL (Rigaku) and the ICDD powder diffraction database PDF4+ (2021 release). The size of crystallites was calculated from XRD peaks broadening using the graphical Halder–Wagner method implemented in the PDXL software package (Rigaku). The approach is based on the graphical representation of the linear relationship $(β/\tanθ)^2$ vs. $β/(\tanθ\sinθ)$ plot (β—XRD peak physical broadening, θ—diffraction angle). The size of the crystallites in the investigated catalysts was determined using the Halder–Wagner method.

The shape and size of palladium and cobalt nanoparticles were examined using a transmission electron microscope Tecnai G2 F20 X-TWIN equipped with an EDAX spectrometer with an r-TEM detector. For microscopic examinations, 10 mg of sample was first sonicated in 1 mL of ethanol for 1 h. Then, the obtained mixture was deposited on the Cu grid covered with a continuous carbon film.

The morphology and composition of the fabricated catalysts were characterized using a SEM/FIB workstation Helios Nanolab 650 with an energy-dispersive X-ray (EDX) spectrometer, INCA Energy 350 X-Max 20.

The composition of the obtained $Pd-Cl_2-Co_3O_4/C$ and $PdOCo_3O_4/C$ was determined by means of X-ray photoelectron spectroscopy (XPS) using an "ESCALABMKII" spectrometer (VG Scientific, East Grinstead, UK) equipped with an Al Kα X-ray radiation source (1486.6 eV) operated at fixed pass energy of 20 eV.

To confirm the palladium and cobalt content, an ICP-OES analysis was conducted. The ICP optical emission spectra were recorded using an ICP optical emission spectrometer Optima 7000DV (Perkin Elmer, Waltham, MA, USA).

3.4. Electrochemical Measurements

All electrochemical measurements were performed with a Metrohm Autolab potentiostat (PGSTAT100) with a rotating disk electrode (RDE) system using the Electrochemical Software (Nova 1.6.013). The 100 mL three-electrode cell was used. The geometric area of the working electrode was 0.07 cm^2. As a counter electrode, a Pt sheet was used, and Ag/AgCl/KCl electrode was used as a reference electrode. The catalyst layer on the

electrode was obtained according to the following steps: firstly, 5 mg of the investigated catalysts were dispersed ultrasonically for 1 h in a 200 μL 2% polyvinylidene fluoride in N-methyl-2-pyrrolidone (PVDF) solution. Then 5 μL of the prepared suspension mixture was pipetted onto the polished surface of the glassy carbon electrode and dried in an oven at 80 °C for 4 h.

The cyclic voltammetry (CV) measurements were recorded in an Ar-deaerated 0.5 M H_2SO_4 solution. The potential was cycled in a range of 0–1.5 V with a scan rate of 50 mV s^{-1}. Linear-sweep voltammograms (LSVs) were recorded on the investigated catalysts in the O_2-saturated 0.1 M NaOH solution, using the rotating disc electrode (RDE) at a scan rate of 5 mV s^{-1}. The rotation rate varied from 0 to 2000 rpm. Chronoamperometric measurements (CA) for ORR were performed at a potential value of 0.55 V in an O_2-saturated 0.1 M NaOH solution for 30 min. The electrode potential values for ORR were quoted versus the reversible hydrogen electrode (RHE).

After measurements, the electron transfer number was calculated using the Koutecky–Levich (K-L) Equations (1)–(3):

$$j^{-1} = j_k^{-1} + j_d^{-1} \tag{1}$$

$$j_d = 0.62 \; nFD^{2/3} \; Co_2 V^{-1/6} \omega^{1/2} \tag{2}$$

$$j^{-1} = j_k^{-1} + w^{-1/2} \times A \tag{3}$$

where, j, j_k and j_d are the measured current density, kinetic current density and the diffusion limiting current density (mA cm^{-2}), respectively; n is the number of electrons transferred in the reaction; F is the Faraday constant; D is the diffusion coefficient of the reactant; Co_2 is the concentration of the reactant in the bulk electrolyte; V is the kinetic viscosity of the electrolyte; w is the rotation rate; A is the slope of the linear plot of j^{-1} versus $w^{-1/2}$ (K-L plot) [44].

All electrochemical measurements were carried out at the temperature of 20 °C. All solutions were deaerated with Ar before each measurement, except ORR measurements. The presented current densities are normalized with respect to the geometric area (0.07 cm^2) of the working electrode.

4. Conclusions

The Co_3O_4/C substrate was prepared using the microwave heating method. Furthermore, the substrate was impregnated with palladium—Pd-Cl$_2$-Co$_3$O$_4$/C. After annealing of Co_3O_4/C and Pd-Cl$_2$-Co$_3$O$_4$/Cat 400 °C for 3 h, Co_3O_4/C-T and PdOCo$_3$O$_4$/C catalysts were obtained. It was determined that annealing improves the electrocatalytic properties of synthesized catalysts.

It was found that Pd-supported catalysts show noticeably greater electrocatalytic activity towards oxygen reduction reaction in the alkaline medium as compared to bare Co_3O_4/C catalysts. Moreover, PdOCo$_3$O$_4$/C catalyst, having up to 3 times lower noble metal loading and remarkably lower ESA compared to the commercial Pt/C, demonstrated even higher electrocatalytic activity for oxygen reduction to commercial Pt/C. The highest activity of PdOCo$_3$O$_4$/C catalyst can be attributed to the synergistic effect between PdO and Co_3O_4.

We think that Co_3O_4/C catalysts impregnated with palladium could be promising electrocatalytic materials able to replace Pt-supported catalysts.

Author Contributions: Conceptualization, V.K. and R.S.; methodology, V.P., V.J. and J.V.; software, V.K. and R.S.; formal analysis, Z.S., R.S. and S.R.; investigation, R.S. and S.R.; validation, V.K. and Z.S.; writing—original draft preparation, V.K.; writing—review and editing, E.N., R.V. and L.T.-T. All authors have read and agreed to the published version of the manuscript.

Data Availability Statement: Not applicable.

References

1. A 1912 News Article Ominously Forecasted the Catastrophic Effects of Fossil Fuels on Climate Change. Available online: https://qz.com/817354/scientists-have-been-forecasting-that-burning-fossil-fuels-will-cause-climate-change-as-early-as-1882/ (accessed on 7 April 2022).
2. Ogungbemi, E.; Ijaodola, O.; Khatib, F.N.; Wilberforce, T.; Hassan, Z.E.; Thompson, J.; Ramadan, M.; Olabid, A.G. Fuel cell membranes-Pros and cons. *Energy* **2019**, *172*, 155–172. [CrossRef]
3. Sui, S.; Wang, X.; Zhou, X.; Su, Y.; Riffat, S.; Liu, C.-J. A comprehensive review of Pt electrocatalysts for the oxygen reduction reaction: Nanostructure, activity, mechanism and carbon support in PEM fuel cells. *J. Mater. Chem. A* **2017**, *5*, 1808–1825. [CrossRef]
4. Gu, J.; Zhang, G.-M.; Yao, R.; Yu, T.; Han, M.-F.; Huang, R.-S. High oxygen reduction activity of Pt-Ni alloy catalyst for proton exchange membrane fuel cells. *Catalysts* **2022**, *12*, 250. [CrossRef]
5. Chiodoni, A.; Salvador, G.P.; Massaglia, G.; Belmondo, L.; Munoz-Tabares, J.A.; Sacco, A.; Garino, N.; Castellino, M.; Margarita, V.; Ahmed, D.; et al. Mn_xO_y-based cathodes for oxygen reduction reaction catalysis in microbial fuel cells. *Int. J. Hydrogen Energy* **2019**, *44*, 4432–4441. [CrossRef]
6. Uskaikar, P.H.; Shett, P.N.; Malode, J.S. Electrocatalytic reduction of oxygen on Co_3O_4: Effects of processing method. *Mater. Sci. Technol.* **2018**, *1*, 129–135. [CrossRef]
7. Kumar, R.; Singh, L.; Zularisam, A.W.; Hai, I.F. Potential of porous Co_3O_4 nanorods as cathode catalyst for oxygen reduction reaction in microbial fuel cells. *Bioresour. Technol.* **2016**, *220*, 537–542. [CrossRef]
8. Gunji, T.; Wakabayashi, R.H.; Noh, S.H.; Han, B.; Matsumoto, F.; Di Salvo, F.J.; Abruna, H.D. The effect of alloying of transition metals (M = Fe, Co, Ni) with palladium catalysts on the electrocatalytic activity for the oxygen reduction reaction in alkaline media. *Electrochim. Acta* **2018**, *283*, 1045–1052. [CrossRef]
9. Lee, Y.; Jang, J.; Lee, G.J.; Jeon, O.S.; Kim, H.S.; Hwang, H.J.; Shul, Y.G. Optimization of the Pd-Fe-Mo Catalysts for Oxygen Reduction Reaction in Proton-Exchange Membrane Fuel Cells. *Electrochim. Acta* **2016**, *220*, 29–35. [CrossRef]
10. Xie, X.; Shen, W. Morphology control of cobalt oxide nanocrystals for promoting their catalytic performance. *Nanoscale* **2009**, *1*, 50–60. [CrossRef]
11. Li, Y.; Zhou, M.; Cui, X.; Yang, Y.; Xiao, P.; Cao, L.; Zhang, Y. Hierarchical structures of nickel, cobalt-based nanosheets and iron oxyhydroxide nanorods arrays for electrochemical capacitors. *Electrochim. Acta* **2015**, *161*, 137–143. [CrossRef]
12. Kumar, R.; Singh, L.; Zularisam, A.W. Enhanced oxygen reduction reaction in air-cathode microbial fuel cells using flower-like Co_3O_4 as an efficient cathode catalyst. *Int. J. Hydrogen Energy* **2017**, *42*, 19287–19295. [CrossRef]
13. Ramos-Docampo, M.; Rivas-Murias, B.; Rodriguez-Gonzalez, B.; Salgueirino, V. Thermodynamically driven oxidation–induced Kirkendall effect in octahedron-shaped cobalt oxide nanocrystals. *CrystEngComm* **2017**, *19*, 5542–5548. [CrossRef]
14. Qian, C.; Guo, X.; Zhang, W.; Yang, H.; Qian, Y.; Xu, F.; Qian, S.; Lin, S.; Fan, T. Co_3O_4 nanoparticles on porous bio-carbon substrate as catalyst for oxygen reduction reaction. *Microporous Mesoporous Mater.* **2019**, *277*, 45–51. [CrossRef]
15. Shahid, M.M.; Rameshkumar, P.; Huang, N.M. Morphology dependent electrocatalytic properties of hydrothermally synthesized cobalt oxide nanostructures. *Ceramics Int.* **2015**, *41*, 13210–13217. [CrossRef]
16. Tabong, C.D.; Ondoh, A.M.; Yufanyi, D.M.; Foba, J. Cobalt(II) and Zinc(II) Complexes of Hexamethylenetetramine as Single Source Precursors for their Metal Oxide Nanoparticles. *J. Mater. Sci. Res.* **2015**, *4*, 70–81. [CrossRef]
17. Jia, W.; Li, J.; Lu, Z.; Juan, Y.; Jiang, Y. Synthesis of Honeycomb-Like Co_3O_4 Nanosheets with Excellent Supercapacitive Performance by Morphological Controlling Derived from the Alkaline Source Ratio. *Materials* **2018**, *11*, 1560. [CrossRef]
18. Liang, H.; Raitano, J.M.; Zhang, L.; Chan, S.-W. Controlled Synthesis of Co3O4 Nanopolyhedrons and Nanosheets at Low Temperature. *Chem. Commun.* **2009**, 7569–7571. [CrossRef]
19. Kepenienė, V.; Stagniūnaitė, R.; Tamašauskaitė-Tamašiūnaitė, L.; Pakštas, V.; Jasulaitienė, V.; Léger, B.; Rousseau, J.; Ponchel, A.; Monflier, E.; Norkus, E. Co_3O_4/C and Au supported Co_3O_4/C nanocomposites–Peculiarities of fabrication and application towards oxygen reduction reaction. *Mat. Chem. Phys.* **2020**, *241*, 122332. [CrossRef]
20. Qu, Q.; Zhang, J.H.; Wang, J.; Li, Q.-Y.; Xu, C.-W.; Lu, X. Three-dimensional ordered mesoporous Co_3O_4 enhanced by Pd for oxygen evolution reaction. *Sci. Rep.* **2017**, *7*, 41542. [CrossRef]
21. Zhang, L.Y.; Sui, L.X.; Zhao, L.; Gu, D.M.; Huang, G.S.; Wang, Z.B. Controlling the surface roughness of chain-like Pd nanowires by pH values as excellent catalysts for oxygen reduction reaction. *Int. J. Hydrogen Energy* **2019**, *44*, 6551–6559. [CrossRef]
22. Erikson, H.; Sarapuu, A.; Gullón, S.J.; Tammeveski, K. Recent progress in oxygen reduction electrocatalysis on Pd-based catalysts. *J. Electroanal. Chem.* **2016**, *780*, 327–336. [CrossRef]
23. Xiong, X.; Chen, W.; Wang, W.; Li, J.; Chen, S. Pt-Pd nanodendrites as oxygen reduction catalyst in polymer-electrolyte-membrane fuel cell. *Int. J. Hydrogen Energy* **2017**, *42*, 25234–25243. [CrossRef]
24. Zheng, F.; Zhang, C.; Gao, X.; Du, C.; Zhuang, Z.; Chen, W. Immobilizing Pd nanoclusters into electronically conductive metal-organic frameworks as bi-functional electrocatalysts for hydrogen evolution and oxygen reduction reactions. *Electrochim. Acta* **2019**, *306*, 627–634. [CrossRef]
25. Liao, M.; Li, W.; Xi, X.; Luo, C.; Fu, Y.; Gui, S.; Mai, Z.; Yan, H.; Jiang, C. Highly active Pt decorated Pd/C nanocatalysts for oxygen reduction reaction. *Int. J. Hydrogen Energy* **2017**, *42*, 24090–24098. [CrossRef]
26. Hoflund, B.; Li, Z. Surface characterization study of a Pd/Co_3O_4 methane oxidation catalyst. *Appl. Surf. Sci.* **2006**, *253*, 2830–2834. [CrossRef]

27. Yang, N.; Ni, S.; Sun, Y.; Zhu, Y. A facial strategy to synthesize Pd/Co$_3$O$_4$nanosheets with enhanced performance for methane catalytic oxidation. *Mol. Catal.* **2018**, *452*, 28–35. [CrossRef]

28. Angerstein-Kozlowska, H.; Conway, B.E.; Sharp, W.B.A. The real condition of electrochemically oxidized platinum surfaces: Part I. Resolution of component processes. *J. Electroanal. Chem.* **1973**, *43*, 9–36. [CrossRef]

29. Grden, M.; Łukaszewski, M.; Jerkiewicz, G.; Czerwinski, A. Electrochemical behaviour of palladium electrode: Oxidation, electrodissolution and ionic adsorption. *Electrochim. Acta.* **2008**, *53*, 7583–7598. [CrossRef]

30. Kepenienė, V.; Tamašauskaitė-Tamašiūnaitė, L.; Vaičiūnienė, J.; Pakštas, V.; Norkus, E. PtCeO$_2$/C and PtNb$_2$O$_5$/C as electrocatalysts for ethanol oxidation. *Chemija* **2016**, *27*, 31–36.

31. Jolm, F.; William, M.F.; Peter, S.E. *SobolKennetlf D. Bomben. Handbook of X-ray Photoelectron Spectroscopy*; Perkin-Elmer Corporation: Minesota, MN, USA, 1992.

32. Militello, M.C.; Simko, S.J. NIST Standard Reference Database 20, Version 4.1, Web Version. *Surf. Sci. Spectra* **1994**, *3*. Available online: http://srdata.nist.gov/xps/ (accessed on 12 July 2022).

33. Yao, X.; Xin, X.; Zhang, Y.; Wang, J.; Liu, Z.; Xu, X. Co$_3$O$_4$ nanowires as high capacity anode materials for lithium ion batteries. *J. Alloy Compd.* **2012**, *521*, 95–100. [CrossRef]

34. Jin, Y.; Wang, L.; Shang, Y.; Gao, J.; Li, J.; He, X. Facile synthesis of monodisperse Co$_3$O$_4$ mesoporous microdisks as an anode material for lithium ion batteries. *Electrochim. Acta* **2015**, *151*, 109–117. [CrossRef]

35. Mc Intyre, N.S.; Johnston, D.D.; Coatsworth, L.L.; Davidson, R.D.; Brown, J.R. NIST Standard Reference Database 20, Version 4.1, Web Version. *Surf. Interface Anal.* **1990**, *15*, 265.

36. Hsieh, P.-T.; Chen, Y.-C.; Kao, K.S.; Wang, C.M. Luminescence mechanism of ZnO thin film investigated by XPS measurement. *Appl. Phys. A* **2008**, *90*, 317–321. [CrossRef]

37. Zhu, Y.; Yue, M.; Natarajan, V.; Kong, L.; Ma, L.; Zhang, Y.; Zhao, Q.; Zhan, J. Efficient activation of persulfate by Fe$_3$O$_4$@β-cyclodextrin nanocomposite for removal of bisphenol A. *RSC Adv.* **2018**, *8*, 14879–14887. [CrossRef]

38. Shi, K.-M.; Cheng, X.; Jia, Z.-Y.; Guo, J.-W.; Wang, C.; Wang, J. Oxygen reduction reaction of Fe-polyaniline/carbon nanotube and Pt/C catalysts in alkali media. *Int. J. Hydrogen Energy* **2016**, *41*, 16903–16912. [CrossRef]

39. Ge, X.; Sumboja, A.; Wuu, D.; An, T.; Li, B.; Goh, T.F.W.; Hor, A.T.S.; Zong, Y.; Liu, Z. Oxygen reduction in alkaline media: From mechanisms to recent advances of catalysts. *ACS Catal.* **2015**, *5*, 4643–4667. [CrossRef]

40. He, Q.; Li, Q.; Khene, S.; Ren, X.; López-Suárez, F.E.; Lozano-Castelló, D.; Bueno-López, A.; Wu, G. High-loading cobalt oxide coupled with nitrogen-doped graphene for oxygen reduction in anion-exchange-membrane alkaline fuel cells. *J. Phys. Chem. C.* **2013**, *117*, 8697–8707. [CrossRef]

41. Wang, Y.; Ma, X.; Lu, L.; He, Y.; Qi, X.; Deng, Y. Carbon supported MnO$_x$-Co$_3$O$_4$ as cathode catalyst for oxygen reduction reaction in alkaline media. *Int. J. Hydrogen Energy* **2013**, *38*, 13611–13616. [CrossRef]

42. Wang, T.; Chutia, A.; Brett, D.J.L.; Shearing, P.R.; He, G.; Chai, G.; Parkin, I.P. Palladium alloys used as electrocatalysts for the oxygen reduction reaction. *Energy Environ. Sci.* **2021**, *14*, 2639–2669. [CrossRef]

43. Hu, T.; Wang, Y.; Zhang, L.; Tang, T.; Xiao, H.; Chen, W.; Zhao, M.; Jia, J.; Zhu, H. Facile synthesis of PdO-doped Co$_3$O$_4$ nanoparticles as an efficient bifunctional oxygen electrocatalyst. *App. Catal. B Environ.* **2019**, *243*, 175–182. [CrossRef]

44. Paulus, U.; Schmidt, T.; Gasteiger, H.; Behm, R. Oxygen reduction on a high-surface area Pt/Vulcan carbon catalyst: A thin-film rotating ring-disk electrode study. *J. Electroanal. Chem.* **2001**, *495*, 134–145. [CrossRef]